

Article

Synthesis and Spectral, Thermal and Antimicrobial Investigation of Mixed Ligand Metal Complexes of *N*-Salicylidene Aniline and 1,10-Phenanthroline

Amira A. Mohamed ¹, Abeer A. Nassr ², Sadeek A. Sadeek ² and Hazem S. Elshafie ^{3,*}¹ Department of Basic Science, Zagazig Higher Institute of Engineering and Technology, Zagazig 44519, Egypt² Department of Chemistry, Faculty of Science, University of Zagazig, Zagazig 44519, Egypt³ School of Agricultural, Forestry, Food and Environmental Sciences, University of Basilicata, Viale dell'Ateneo Lucano, Potenza 85100, Italy

* Correspondence: hazem.elshafie@unibas.it; Tel.: +39-0971-205498; Fax: +39-0971-205503

Abstract: Coordination compounds of Co(II), Cu(II), Y(III), Zr(IV) and La(III) ions were synthesized from the *N*-salicylidene aniline (**L**) derived from the condensation of aniline with salicylaldehyde and 1,10-phenanthroline (**phen**) as a secondary mixed ligand. **L**, **phen** and their complexes were characterized using various physicochemical methods, such as elemental analyses (CHN), Fourier-transform infrared spectroscopy (FT-IR), molar conductance (Λ), magnetic susceptibility (μ_{eff}), proton nuclear magnetic resonance (^1H NMR), ultraviolet–visible spectroscopy (UV–Vis) and thermogravimetric analysis (TG/DTG). The analytical and spectroscopic data supporting the chemical formulas of the metal complexes and chelation of **L** and **phen** with the metal ions forming octahedral complexes. FT-IR spectra demonstrated that **L** chelated with metal ions as a bidentate ligand via the oxygen atom of the phenolic group with a band in the range 3378–3437 cm^{-1} and the nitrogen atom of the azomethine group at 1612 cm^{-1} . In addition, **phen** chelated through two nitrogen atoms in the range 1525–1565 cm^{-1} . The ^1H NMR results confirmed the IR assumption that the ligand connected to the metal ions via the phenolic's oxygen atom. The molar conductance measurements of the complexes revealed high values of the electrolytic nature of these complexes in the range of 90.40–125.80 $\text{S cm}^2 \text{mol}^{-1}$. Thermal analysis (TG/DTG) was used to differentiate between coordinated and hydrated water molecules and the thermal stability of the complexes. Finally, the anti-microbial activities of the complexes were investigated against fungi (*Candida albicans*), Gram-negative bacteria (*Escherichia coli* and *Salmonella typhimurium*) and Gram-positive bacteria (*Staphylococcus aureus* and *Micrococcus* sp.) using the disc diffusion method. The La(III) complex was significant against *C. albicans* compared with all other compounds and reference standard control.

Keywords: mixed ligand complexes; ^1H NMR; TG/DTG; UV–visible; biological activity

Citation: Mohamed, A.A.; Nassr, A.A.; Sadeek, S.A.; Elshafie, H.S. Synthesis and Spectral, Thermal and Antimicrobial Investigation of Mixed Ligand Metal Complexes of *N*-Salicylidene Aniline and 1,10-Phenanthroline. *Compounds* **2023**, *3*, 298–309. <https://doi.org/10.3390/compounds3010022>

Academic Editor: Juan C. Mejuto

Received: 31 January 2023

Revised: 21 February 2023

Accepted: 13 March 2023

Published: 16 March 2023

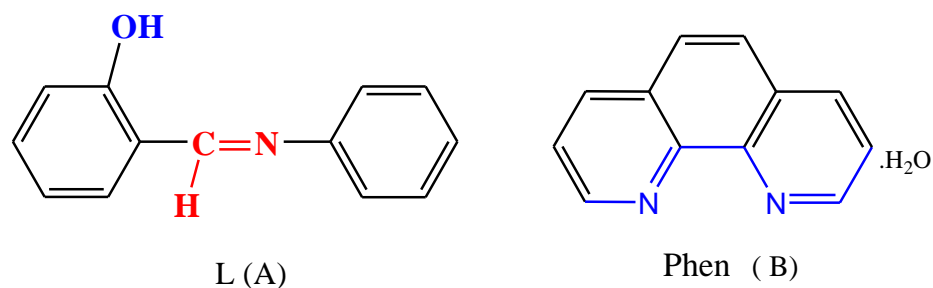


Copyright: © 2023 by the authors. Licensee MDPI, Basel, Switzerland. This article is an open access article distributed under the terms and conditions of the Creative Commons Attribution (CC BY) license (<https://creativecommons.org/licenses/by/4.0/>).

1. Introduction

Schiff base ligands contain N, O donor atoms that may be used in the reduction reaction of ketones, and oxidation of organic compounds, dyes, pigments, catalysts and polymers [1–3]. Schiff base chelated with metal ions forms stable complexes employed in biological, analytical, agricultural, industrial, and medicinal applications [3,4]. There are imine or azomethine groups in a number of natural, naturally derived, and synthetic substances. Such compounds are demonstrated to be crucial to their biological functions [5–10]. The first-row transition metals, in particular cobalt and copper, are significant to biology because they are linked to a variety of proteins that are crucial for vital physiological functions [11–15]. The prolate-shaped *N*-salicylidene anilines (Scheme 1A) belong to the class of liquid crystals with rod- and disc-shaped structural units [16–20] that have undergone extensive study and are employed in a wide range of scientific, technological, industrial domains and possess mesomorphism that have photochromic properties [21–23]. Some

metals, such as Co, Ni, Cu, Rh, Pd and Pt, combine with *N*-salicylidene anilines, and the resulting complexes modify the geometric structure of molecules and exhibit smectic mesomorphism [24–26]. **Phen** (Scheme 1B) is a powerful nitrogen donor ligand that effectively chelates metal ions to form stable complexes and has supplemental features for complexes due to it possessing heteroaromatic and aromatic groups [27,28].



Scheme 1. Structural formulae of (A) L *N*-salicylidene aniline and (B) 1,10-phenanthroline (**phen**).

The objectives of this research were to investigate the effects of changing atomic volume, atomic mass, and oxidation state of Co(II), Cu(II), Y(III), Zr(IV) and La(III) on the biological activity of the parent ligand (L) in presence of **phen**. These unique electrolytic mononuclear metal complexes have been subjected to spectroscopic characterization using spectroscopic techniques, such as FT-IR, UV-Vis, ^1H NMR, CHN, molar conductivity, magnetic susceptibility studies and thermal analyses. These compounds' antimicrobial efficacy has been assessed in vitro against bacteria and fungi, as well as statistical analysis of the antimicrobial data.

2. Experimental Section

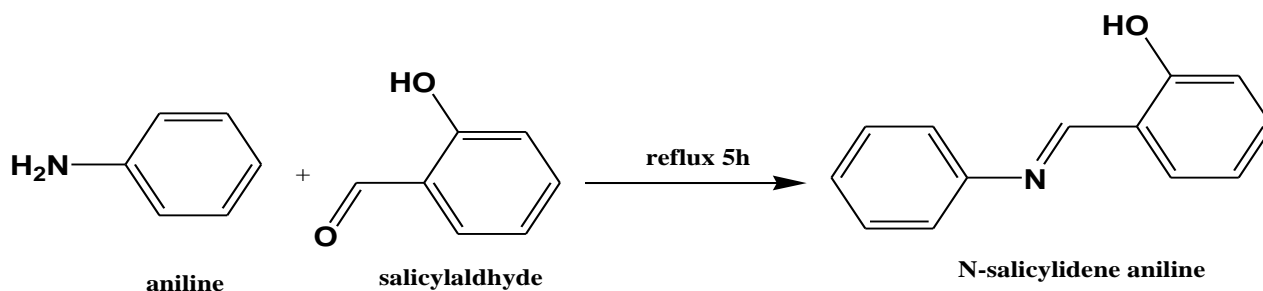
2.1. Materials and Instruments

The highest purity analytical grade chemicals were used for all applications. Salicylaldehyde, aniline, **phen**, ethanol absolute, dimethylformamide (DMF), dimethyl sulfoxide (DMSO), cobalt chloride hexahydrate, copper chloride dihydrate, yttrium chloride hexahydrate, zirconium chloride octahydrate, lanthanum chloride heptahydrate, potassium chromate, concentrated sulfuric acid and silver nitrate from sigma, Aldrich and Fluka Chemical Co. All glasswares were submerged in a chromatic solution ($\text{K}_2\text{Cr}_2\text{O}_7$ + concentrated H_2SO_4) before being thoroughly washed with bidistilled water and dried in an oven at $100\text{ }^\circ\text{C}$.

The range of $4000\text{--}400\text{ cm}^{-1}$ of the FT-IR spectra in KBr discs was recorded by using FT-IR 460 PLUS Spectrophotometer. DMSO-*d*₆ was employed as the solvent to acquire the ^1H NMR spectra on a Varian Mercury VX-300 NMR Spectrometer. UV-3101PC Shimadzu completed the electronic spectra. The absorption spectra were recorded as DMSO solutions. Shimadzu TGA-50H was used for implementation. TG-DTG measurements were performed in an environment of N_2 at temperatures ranging from ambient $^\circ\text{C}$ to $1000\text{ }^\circ\text{C}$, and the sample mass was meticulously weighed out in an aluminum crucible. To quantify the M percent content, three analytical methods were used. This purposeful experiment included complexometric titration, thermogravimetry by converting the solid products into metal oxide, and atomic absorption utilizing a spectrometer type PYE-UNICAM SP 1900 equipped with the appropriate lamp [29,30]. The percent of CHN was carried out using a Perkin Elmer 2400 CHN elemental analyzer. Melting points were measured on a Buchi device. With a Gouy balance and $\text{Hg}[\text{Co}(\text{CSN})_4]$ as the signing material, the magnetic susceptibilities of the powdered materials were investigated on a Sherwood scientific magnetic scale. Using CONSORT K410, the molar conductance of $1 \times 10^{-3}\text{ M}$ solutions of the ligands and their complexes in DMF was examined. Each experiment used freshly made solutions and was conducted at room temperature.

2.2. Preparation of *N*-Salicylidene Aniline (**L**)

Light yellow solid compound (**L**) was obtained by the reaction of 20 mmol aniline (1.82 mL) with 10 mmol of salicylaldehyde (2.08 mL) (Scheme 2) using absolute ethanol and refluxed with constant stirring for 5 h in presence of 1 mL glacial acetic acid and concentrated to 8 mL in a water bath and allowed to cool at 0 °C. The formed precipitate was filtered off and dried over anhydrous CaCl₂.



Scheme 2. Preparation of *N*-salicylidene aniline (**L**).

2.3. Synthesis of Metal Complexes

The dark green solid complex [Co(**L**)(**phen**)(H₂O)₂]₂Cl₂·6H₂O (**1**) was created by combining 1 mmol of **L** (0.197 g) with 1 mmol of **phen** (0.198 g) in 20 mL of ethanol. After 10 min of stirring the mixture, we added 1 mmol (0.237 g) of CoCl₂·6H₂O in 20 mL ethanol dropwise and refluxed for 6 h. The dark green precipitate was dried over anhydrous CaCl₂ under vacuum. Dark brown complex [Cu(**L**)(**phen**)(H₂O)₂]₂Cl₂ (**2**), dark blue [Y(**L**)(**phen**)(H₂O)₂]₃·5H₂O (**3**), green [ZrO(**L**)(**phen**)(H₂O)]Cl₂ (**4**) and yellow [La(**L**)(**phen**)(H₂O)₂]₃ (**5**) were made in a similar way to that previously described, using ethanol. CoCl₂·6H₂O, YCl₃·6H₂O, ZrOCl₂·8H₂O, LaCl₃·7H₂O, respectively in 1:1:1 (**L**:**phen**:M) molar ratio.

2.4. Antimicrobial Investigation

Five standard microbial strains, two Gram-negative bacteria (*Escherichia coli* ATCC 10536 and *Salmonella typhimurium* ATCC 14028), two Gram-positive bacteria (*Staphylococcus aureus* ATCC 6538 and *Micrococcus* sp. TCC 10240) and one fungi (*Candida albicans* ATCC 10231) were obtained as pure cultures from the microbial collection of the School of Agricultural, Forestry, Food and Environmental Sciences (SAFE), University of Basilicata, Potenza, Italy. The antimicrobial activity of the tested samples was determined at the Laboratory of Phytopathology, SAFE, University of Basilicata by using the disc diffusion method according to Clinical Laboratory and Standards Institute Guidelines [31,32] (CLSI, 2012). The microbial strains were inoculated into Mueller-Hinton broth and incubated at 35 °C until it reached a turbidity equivalent to or greater than that of the 0.5 McFarland standard. The turbidity of the suspension was adjusted with sterile saline to achieve a turbidity equivalent to that of a 0.5 McFarland standard. Sterile Mueller–Hinton agar plates were poured aseptically. A sterile cotton swab should ideally be dipped into the modified suspension within 15 min of altering the inoculum suspension's turbidity. The swab should be turned around many times and firmly pressed against the interior tube wall above the fluid level. By doing this, the swab's extra inoculum will be removed. By streaking the swab across the whole sterile agar surface of a Mueller-Hinton agar plate's dried surface, the plate is infected. To ensure an evenly distributed inoculum, streak the plate two more times while rotating it by about 60 degrees each time. The rim of the agar is swabbed as a last step. Before using the drug-impregnated discs, the lid may be left open for 3 to 5 min, but no longer than 15 min, to allow any excess surface moisture to be absorbed. To ensure full contact with the agar surface, sterile filter paper discs of about 5 mm in diameter that were impregnated with 8 L of the test samples were placed on the plates. The diameter of the inhibitory zones was determined after the plates were inverted and incubated at 37 °C for 16 to 20 h [31,33,34]. Inhibition of microbial growth was calculated in relation to the

positive control. Using the equation, the compounds' activity index percent was calculated. The whole experiment was carried out twice with three replicates, and the obtained data are illustrated as mean values \pm SDs.

$$\% \text{ Activity Index} = \frac{\text{Zone of inhibition by test compound (diameter)}}{\text{Zone of inhibition by standard (diameter)}} \times 100 \quad (1)$$

3. Results and Discussion

The physical characteristics and the analytical data of our complexes are mentioned in Table 1, and, according to the obtained data, the complexes are formed of 1:1:1 (**L:phen:Metal**) stoichiometry. All the complexes are hydrates except Zr(IV) complex with high melting points, air-stable at room temperature and insoluble in most organic solvents but soluble in DMF and DMSO mediums. The molar conductance measurements in 10^{-3} M DMF of **1**, **3**, **4** and **5** complexes are in 90.40–125.80 $\Omega \text{ cm}^2 \text{ mol}^{-1}$ range; these high values revealed the electrolytic nature of these complexes [35,36]. Qualitative data demonstrated the existence of chloride within the complex sphere.

Table 1. Elemental analysis and Physico-analytical data for **L**, **Phen** and their complexes.

Compounds M.Wt. (M.F)	Yield%	Mp/ $^{\circ}$ C	Color	(Calcd.) Found (%)					Λ ($\text{S cm}^2 \text{ mol}^{-1}$)
				C	H	N	Cl	M	
L 197 ($\text{C}_{13}\text{H}_{11}\text{NO}$)	-	50 (49–51)	Light-yellow	(79.18) 79.01	(5.58) 5.52	(7.10) 6.89	-	-	1.45
Phen 198.23 ($\text{C}_{12}\text{H}_{10}\text{N}_2\text{O}$)	-	100	White	(72.64) 72.59	(5.04) 4.87	(14.12) 14.03	-	-	5.00
(1) 650.933 ($\text{CoC}_{25}\text{H}_{35}\text{N}_3\text{O}_9\text{Cl}_2$)	90.02	>300	Dark-green	(46.08) 45.92	(5.37) 5.24	(6.45) 6.19	(10.90) 10.88	(9.05) 8.99	95.80 (94.81–96.80)
(2) 547.56 ($\text{CuC}_{25}\text{H}_{23}\text{N}_3\text{O}_3\text{Cl}_2$)	88.22	213 (212–214)	Dark-brown	(54.78) 54.72	(4.20) 4.14	(7.67) 7.62	(12.94) (12.88)	(11.60) 11.52	90.40 (88.60–92.21)
(3) 698.4 ($\text{YC}_{25}\text{H}_{33}\text{N}_3\text{O}_8\text{Cl}_3$)	91.34	220 (219–221)	Dark-blue	(42.95) 42.83	(4.72) 4.57	(6.01) 5.86	(15.24) 15.18	(12.72) 11.69	120.51 (119.20–121.83)
(4) 573.334 ($\text{ZrC}_{25}\text{H}_{21}\text{N}_3\text{O}_3\text{Cl}_2$)	85.69	>300	Green	(52.32) 52.22	(3.66) 3.56	(7.32) 7.22	(12.36) 12.25	(15.91) 15.81	93.70 (92.69–94.71)
(5) 658.4 ($\text{LaC}_{25}\text{H}_{23}\text{N}_3\text{O}_3\text{Cl}_3$)	89.12	>300	Yellow	(45.56) 45.41	(3.49) 3.40	(6.37) 6.31	(16.15) 16.11	(21.09) 21.02	125.80 (124.90–126.70)

3.1. FT-IR Spectra

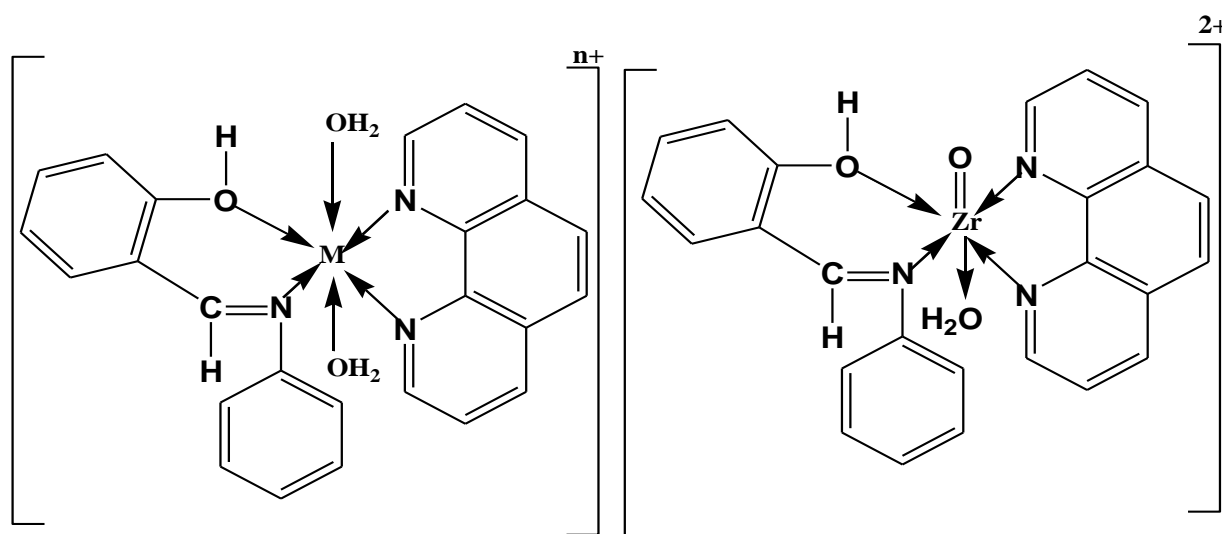
To monitor the complexation of the transition metal ions by the organic ligand, FT-IR spectroscopy can be a useful analytical technique. To verify the mixed ligand's mechanism of binding to the appropriate metal ions in the complexes, the FT-IR spectra of **L** and **phen** were compared to those of the metal complexes (Figure S1). We initially paid attention to the vibrations of the metal complexes, phenolic and azomethine groups because this supports the mechanism that was hypothesized for the interaction between **L** and the metal cations. The broad and medium intensity bands observed in the range 3378–3437 cm^{-1} (Table 2) in FT-IR spectra of complexes are assigned to O–H stretching vibrations of the phenolic group, lattice and coordinated water [11–14,37]. The chelation mode and structures of complexes are shown in Scheme 3. According to the provided information, $\nu(\text{Zr}=\text{O})$ is a medium band at 846 cm^{-1} [38]. The vibrational mode $\nu(\text{C}=\text{N})$ of azomethine group for **L** was visible at 1612 cm^{-1} ; this band shifted to lower frequencies around 1600 cm^{-1} in all metal complexes, which indicates chelation with the metal [13,14]. **Phen** was matched with metal ions through the two nitrogen atoms and displayed bidentate ligand behavior, as evidenced by the free **phen** peak at 1586 cm^{-1} . After chelation, this peak shifted to lower values at 1525–1565 cm^{-1} [37,38]. The decrease of $\nu(\text{C}=\text{N})$ resulted from the decrease in the stretching force constant of the C=N bond as a consequence of the coordination of the nitrogen atom of the azomethine group to the metal ions [39–42]. New bands with varying intensities at 758, 663 cm^{-1} for complex **(1)**, at 756, 621 cm^{-1} for complex **(2)**, at 726, 657 cm^{-1} , for complex **(3)**, at 756, 652 cm^{-1} for complex **(4)** and at 721, 630 cm^{-1} for

complex (5), which are absent in the spectra of **L** and **phen** indicate the chelation of **L** and **phen** with metal ion [43–45].

Table 2. Infrared wavenumber (cm^{-1}) of **L**, **phen** and their complexes.

L	phen	(1)	(2)	(3)	(4)	(5)	Assignments
3426 mbr	3380 sbr	3433 mbr	3426 mbr	3378 mbr	3390 mbr	3437 ms	$\nu(\text{O-H}); \text{H}_2\text{O}$
1612 vs		1600 vs	1605 vs	1601 s	1600 vs	1602 sh	$\nu(\text{C=N})$ of azomethine group
	1586 ms	1526 m	1527 ms	1565 w	1526 m	1525 m	$\nu(\text{C=N})$ pyridine ring
		758 s	756 s	726 w	756 s	721 vs	$\nu(\text{M-O})$ and $\nu(\text{M-N})$
		663 vw	621 w	657 m	652 sh	630 m	

Keys: s = strong, w = weak, v = very, m = medium, br = broad, sh = shoulder, ν = stretching.



Scheme 3. The chelation mode of **L**, **phen** with Co(II), Cu(II), Zr(IV), Y(III) and La(III) metals ion. M = Co(II), Cu(II) for $n = 2$ and M = La(III) and Y(III) for $n = 3$.

3.2. Electronic Spectra and Magnetic Moment Measurements

UV–visible spectral data for **L**, **phen** and their mixed complexes were recorded in the wavelength range 200–800 nm in DMSO solvent. The intra-ligand transitions ($\pi-\pi^*$ and $n-\pi^*$) for **L** were accountable at 270, 302, 318 and 340 nm (Figure S2) and Table 3 [11,12]. In addition, **phen** shows bands at 273, 310 and 350 nm, which may be assigned to $\pi-\pi^*$ and $n-\pi^*$ transitions [13,14,37,38]. The shifting of the absorption bands of $\pi-\pi^*$ and $n-\pi^*$ to higher or lower frequencies indicates the formation of complexes. For our complexes, the presence of new peaks in the range 460–480 nm may be assigned to ligand–metal charge transfer [46]. Co(II) complex's electronic spectrum exhibits an absorption band at $16,528 \text{ cm}^{-1}$, which equates to ${}^4\text{T}_{1g}(\text{F}) \rightarrow {}^4\text{T}_{1g}(\text{P})$ transitions, and a noticeable magnetic moment estimate of 5.11 B.M, demonstrating that the complex seems to have a high spin octahedral with 10 dq 198 kJ/mole and CFSE $198+2p$ [45,46]. The band observed at $17,241 \text{ cm}^{-1}$ for Cu(II) complex may be assigned to ${}^2\text{B}_{1g} \rightarrow {}^2\text{E}_g$ transition [11–14,47,48], the magnetic moment of the complex at 1.70 B. M, which was within the typical range for octahedral Cu(II) complexes with 10 dq 206 kJ/mole and CFSE $206+4p$ [47]. No d–d transitions were noticed for the complexes Y(III), Zr(IV), and La(III) since these complexes are diamagnetic as expected given their electron configuration (d^0). Complexes' molar absorptivity (ϵ), as determined by their electronic spectra, was published (Table 3) utilizing the following equation: $A = \epsilon cl$, where $c = 1 \times 10^{-3} \text{ M}$ and l is the length of the cell (1 cm).

Table 3. UV-Vis. spectra of **L**, **phen** and their complexes.

Compounds	Peak		Assignment	ϵ ($M^{-1}cm^{-1}$) $\times 10^4$	10 Dq		CFSE#	μ_{eff} (B.M)	Postulated Structure
	nm	cm^{-1}			cm^{-1}	kJ/mol			
L	270	37,037	$\pi \rightarrow \pi^*$	0.600					
	302	33,112	$n \rightarrow \pi^*$	0.800					
	318	31,446	$n \rightarrow \pi^*$	0.723					
	340	29,411	$n \rightarrow \pi^*$	0.769					
Phen	273	41,152	$\pi \rightarrow \pi^*$	1.500					
	310	36,630	$n \rightarrow \pi^*$	2.000					
	350	28,571	$n \rightarrow \pi^*$	0.400					
(1)	275	36,363	$\pi \rightarrow \pi^*$	0.912	16,528	198	198+2p	5.11	octahedral
	300	33,333	$n \rightarrow \pi^*$	1.300					
	316	31,645	$n \rightarrow \pi^*$	0.812					
	338	29,585	$n \rightarrow \pi^*$	0.500					
	475	21,052	CT	0.423					
	605	16,528	${}^4T_{1g} \rightarrow {}^4E_{1g}$	0.350					
(2)	245	41,666	$\pi \rightarrow \pi^*$	1.320	17,241	206	206+4p	1.70	octahedral
	286	34,965	$n \rightarrow \pi^*$	0.780					
	397	25,188	$n \rightarrow \pi^*$	0.387					
	460	21,739	CT	0.312					
	580	17,241	${}^2B_{1g} \rightarrow {}^2E_{1g}$	0.200					
(3)	250	40,000	$\pi \rightarrow \pi^*$	1.600					octahedral
	275	34,129	$\pi \rightarrow \pi^*$	0.800					
	310	32,258	$n \rightarrow \pi^*$	0.750					
	318	22,123	$n \rightarrow \pi^*$	0.900					
	340	29,411	$n \rightarrow \pi^*$	0.950					
	480	20,833	CT	0.500					
(4)	247	40,485	$\pi \rightarrow \pi^*$	1.200					
	265	37,735	$\pi \rightarrow \pi^*$	1.620					
	346	28,901	$n \rightarrow \pi^*$	0.200					
	465	21,505	CT	0.450					
(5)	244	40,983	$\pi \rightarrow \pi^*$	2.230					octahedral
	275	36,363	$\pi \rightarrow \pi^*$	1.330					
	320	31,250	$n \rightarrow \pi^*$	1.230					
	345	28,985	$n \rightarrow \pi^*$	1.450					
	467	21,413	CT	0.650					

3.3. 1H NMR Spectra

In d6-dimethylsulfoxide (DMSO) solution, the 1H NMR spectra of **L**, **phen** and their complexes were recorded using tetramethylsilane (TMS) as an internal reference (Figure S3) Table 4. The 1H NMR spectrum of **L** and **phen** ligand showed a band at δ : 2.48 corresponding to N=CH aliphatic and at δ : 6.96–8.96 ppm for –CH aromatic [49]. Figure S3 demonstrates a singlet (OH) at δ : 13.09 ppm, which may be assigned to the phenolic OH [50]. It is implied that **L** is coordinated through the oxygen atom of the phenolic proton since the phenolic proton OH is observable in the spectra of the complexes with chemical shift. Due to the presence of water molecules in the complexes, the 1H NMR spectra for all of the complexes reveal a distinct signal in the interval of 3.36–4.35 ppm [50,51]. All signals from the free ligands are evident in the complexes' spectra when compared to **L**, **phen**, with some changes resulting from the ligand's interaction with the metal.

Table 4. H NMR values (ppm) and tentative assignments for **L**, **phen** and their complexes.

L	Phen	(1)	(2)	(3)	(4)	(5)	Assignments
2.48	-	1.98–2.51	1.25–2.50	2.51	1.99–2.53	2.50	δ H, –CH aliphatic
-	3.37	4.35	3.37	3.36	4.17	3.33	δ H, H ₂ O
6.96–8.95	7.26–8.81	7.11–8.95	7.54	7.31–8.96	7.02–8.50	7.00–8.96	δ H, –CH aromatic
13.09	-	13.01	13.00	13.02	14.87	13.00	δ H, –OH

3.4. Thermal Analysis (TG and DTG)

The thermogravimetric analyses (TG and DTG) for **L**, **phen** and their complexes were done. The TG data and their assignments are summarized in Table 5 and displayed in Figure S4. The results of thermal study showed good consistency with the molecular formula obtained from the elemental analysis data. The TG of **L** advanced through one step with an estimated mass loss of 99.68% (calc: as 100.00%) at T_{\max} 200 °C corresponding to $2C_4H_2 + H_2O + 0.5N_2 + 2.5C_2H_2$. The literature review reported the thermal degradation of **phen** at T_{\max} 95 °C with loss weight 8.98% (calc: 9.08%) to loss H₂O. The second step with T_{\max} 278 °C and weight loss of 90.87% (calc: 90.92%) corresponded to the loss of $2C_4H_2 + 2C_2H_2 + N_2$ with activation energy 117.83 kJ/mole [52,53]. Complexes **(1)** and **(3)** have nearly identical thermal behavior and break down with three stages: The first one corresponds to the loss of lattice water molecules at T_{\max} 41 and 85 °C. The second decomposition stage at T_{\max} 172, 285 and 150, 283 °C with loss of $6C_2H_2 + C_2N_2 + H_2O + 2C_4H_2 + 0.5O_2$ and $2H_2O + 12C_2H_2$, respectively. The third step involves decomposition at 330, 432, 657 and 475, 810 °C maxima (Table 5). According to TG curve complexes **(2)**, **(4)** and **(5)** are thermally stable up to 170 °C and then decompose in two steps: The first one of degradation matches to loss of $2H_2O + 4C_2H_2$, $3C_4H_2$ and $2H_2O$ with a mass loss of 25.51% (calc 25.57%), 17.40% (calc 17.44%) and 5.40% (calc 5.47%). The second step corresponds to loss of $4C_4H_2 + CO + 2HCl + 1.5N_2 + 0.5H_2$, $2C_4H_2 + CO + 2HCl + 3NH_3$ and $9C_2H_2 + C_2N_2 + CO + HCN + 1.5Cl_2$ with T_{\max} 495, 530, 428 and 506 °C.

Table 5. The maximum temperature T_{\max} (°C) and weight loss for **L**, **phen** and their complexes.

Compounds	Decomposition	T_{\max} (°C)	Weight Loss (%)		Lost Species
			Calc.	Found	
L	First step	200	100.00	99.68	$2C_4H_2 + H_2O + 0.5N_2 + 2.5C_2H_2$
	Total loss		100.00	99.68	
phen	First step	95	9.08	8.98	H ₂ O
	Second step	278	90.92	90.87	$2C_4H_2 + 2C_2H_2 + N_2$
	Total loss		100	100	
(1)	First step	41	16.59	16.22	6H ₂ O
	Second step	172,258	52.55	52.64	$6C_2H_2 + C_2N_2 + H_2O + 2C_4H_2 + 0.5O_2$
	Third step	330,432,657	15.67	15.80	
	Total loss		84.81	84.66	$CH_4 + 0.5Cl_2 + 0.5N_2 + HCl$
	Residue		15.19	15.34	CoO + 2C
(2)	First step	175,288	25.57	25.51	$2H_2O + 4C_2H_2$
	Second step	495	62.83	62.80	$4C_4H_2 + CO + 2HCl + 1.5N_2 + 0.5H_2$
	Total loss		88.40	88.31	
	Residue	11.60	11.69	Cu	
(3)	First step	85	12.89	12.85	5H ₂ O
	Second step	150,283	49.81	49.79	$2H_2O + 12C_2H_2$
	Third step	475,810	19.41	19.40	$3HCl + 0.5H_2 + 2NO + NO_2 + 0.5H_2O$
	Total loss		82.11	82.04	
	Residue		17.89	17.96	
(4)	First step	220	17.44	17.40	$3C_4H_2$
	Second step	530	52.70	52.80	$2C_4H_2 + CO + 2HCl + 3NH_3$
	Total loss		70.14	70.20	
	Residue	29.86	29.80	ZrO ₂ + 4C	
(5)	First step	174	5.47	5.40	2H ₂ O
	Second step	428,506	67.95	67.88	$9C_2H_2 + C_2N_2 + CO + HCN + 1.5Cl_2$
	Total loss		73.42	73.28	
	Residue		26.58	26.72	

3.5. Antimicrobial Investigation

The antimicrobial property of **L**, **phen**, and their metal complexes versus distinct bacterial and fungal species was assessed utilizing the disc diffusion method. Generally, the findings shown in Figure 1 illustrated that the prepared complexes have promising antifungal and antibacterial properties. Following the revelation that chelating compounds can suppress the development of bacteria when complexed with a variety of metals, the antibacterial properties of transition metal complexes have been specifically explored in great detail. The created compounds were discovered to have exceptional bactericidal properties. However, it is intriguing to note that, as shown in Table 6, when biological activity undergoes complexation with the metal ions, it increases in comparison to the examined standards.

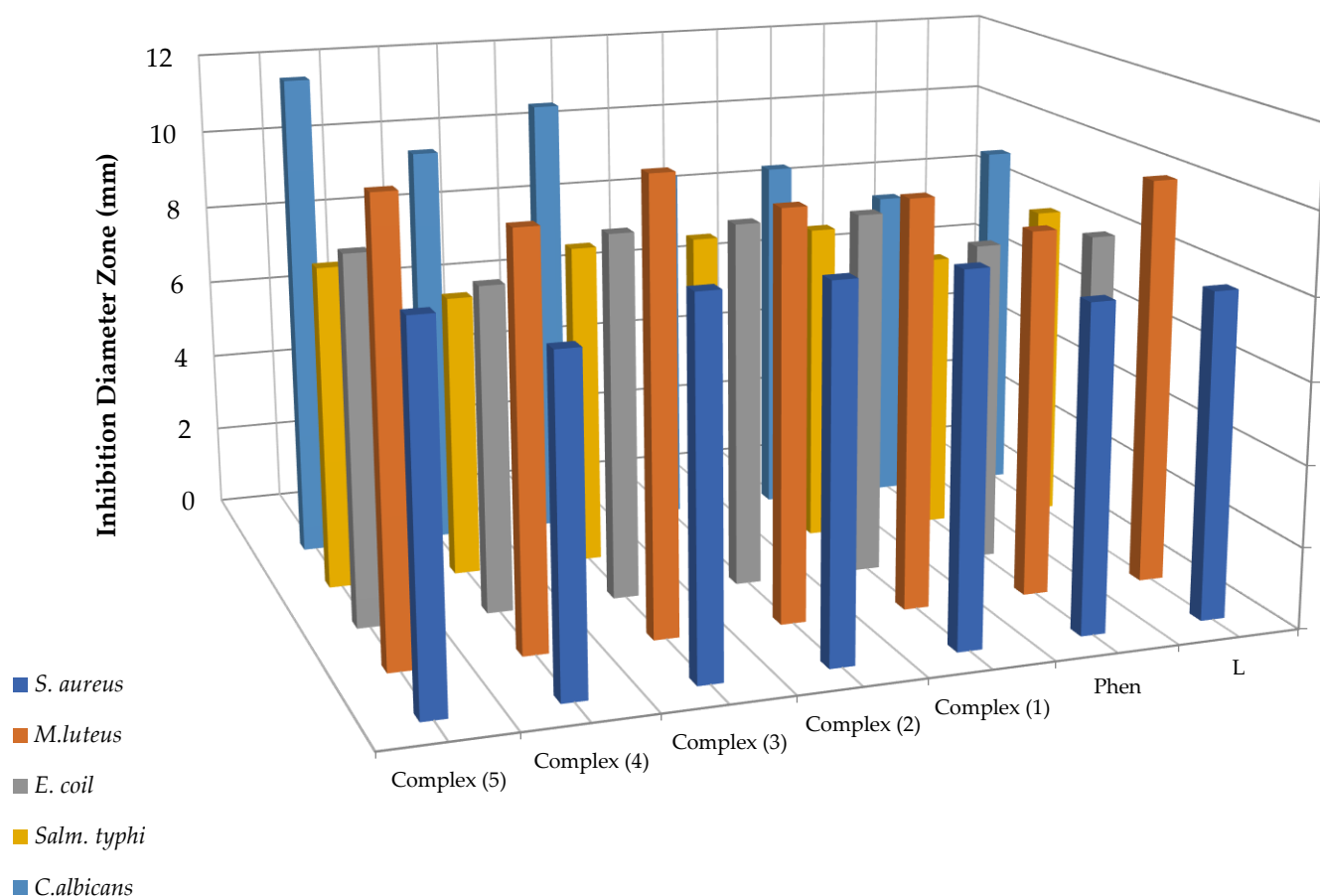


Figure 1. Antimicrobial activity of **L**, **phen** and their complexes.

Regarding the antifungal activity, complex (5) possesses significant activity against *C. albicans* compared to **L** and **phen**. On the basis of chelation theory, this increased activity of the metal complexes can be explained [54,55]. The permeability of the cell membrane and the lipid composition of the studied microbial cells' cell walls enable the easier passage of soluble compounds through the cell, which is a significant aspect of assessing an antimicrobial agent's efficacy [54,55]. This suggests that chelation may facilitate metal complex diffusion across the lipid layer of the cell membrane to the site of action [56–60]. Table 6 and Figure 2 provide measurements of the compounds' activity indices.

Table 6. The inhibition diameter zone (mm) and the activity index (%) values for **L**, **Phen** and their complexes.

Tested Compounds	Tested Microbial Species										
	G(+ve) Bacteria					G(−ve) Bacteria				Fungi	
	<i>S. aureus</i>		<i>M. luteus</i>		<i>E. coli</i>		<i>Salm. typhi</i>		<i>C. albicans</i>		
	D.Iz ^a (mm)	AI ^b (%)	D.Iz (mm)	AI (%)	D.Iz (mm)	AI (%)	D.Iz (mm)	AI (%)	D.Iz (mm)	AI (%)	
L	8 ±0.17	32	10 ±0.08	34.48	8 ±0.12	23.52	8 ±0.14	25	9 ±0.19	50	
Phen	8 ±0.39	32	9 ±0.24	31.03	8 ±0.13	35.52	7 ±0.31	21.87	8 ±0.36	44.44	
(1)	9 ^{NS} ±0.50	36	10 ±0.41	34.48	9 ^{NS} ±0.42	26.47	8 ±0.21	25	9 ±0.44	50	
(2)	9 ^{NS} ±0.48	36	10 ±0.20	34.48	9 ^{NS} ±0.35	26.47	8 ±0.29	25	9 ±0.59	50	
(3)	9 ^{NS} ±0.59	36	11 ^{NS} ±0.32	37.93	9 ^{NS} ±0.52	26.47	8 ±0.40	25	11 ^{NS} ±0.70	61.11	
(4)	8 ±0.18	32	10 ±0.27	34.48	8 ±0.23	23.52	7 ±0.28	21.87	10 ^{NS} ±0.66	55.55	
(5)	9 ^{NS} ±0.64	36	11 ^{NS} ±0.35	37.93	9 ^{NS} ±0.55	26.47	8 ±0.33	25	12 ⁺¹ ±0.37	66.66	
Ciprofloxacin (control)	25 ±0.3	100	29 ±0.2	100	34 ±1.11	100	32 ±0.98	100	0	0	
Nystatin (control)	0	0	0	0	0	0	0	0	18 ±0.42	100	
DMSO (control)	0	0	0	0	0	0	0	0	0	0	
DMF (control)	0	0	0	0	0	0	0	0	0	0	

(a) D.Iz (mm): the diameter of inhibition zone in millimeters. (b) AI (%): the activity index for the tested compounds. (c) (DMF) dimethyl formamide and (DMSO) dimethyl sulfoxide, ⁺¹ significant and ^{NS} not significant.

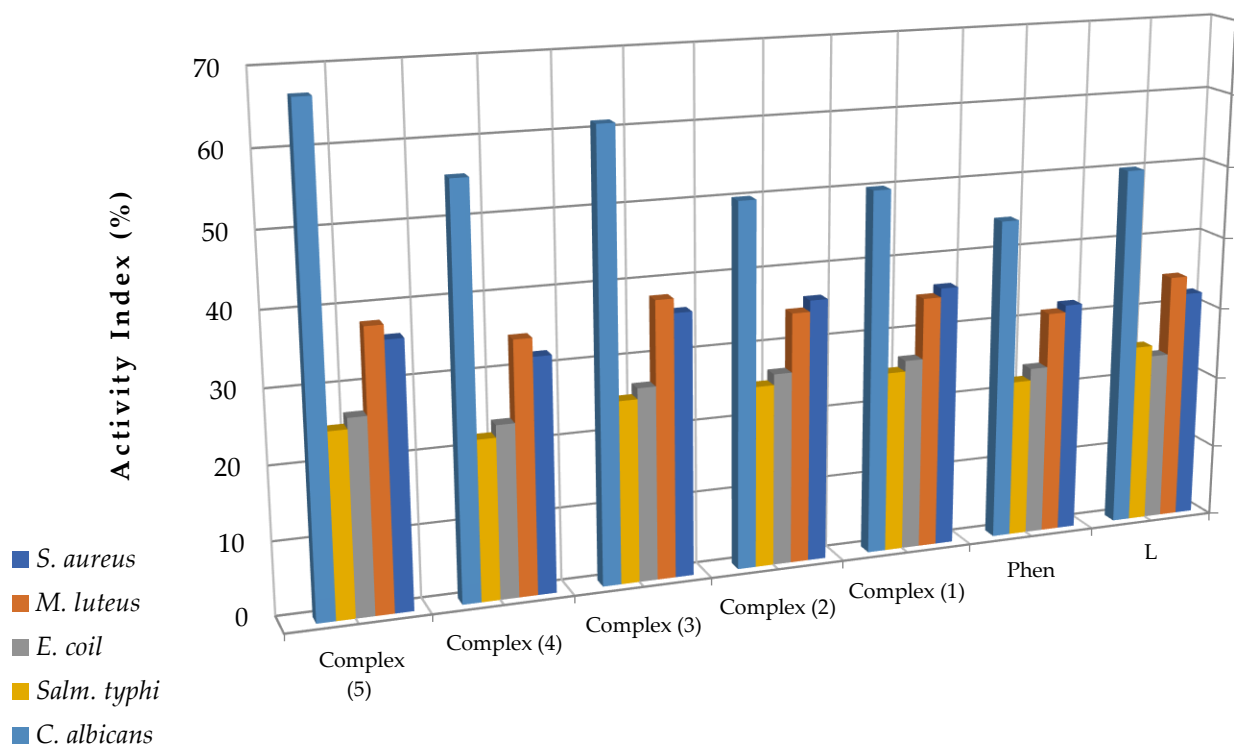


Figure 2. Activity index % for **L**, **phen**, and their complexes.

4. Conclusions

The chelation of oxygen, nitrogen of **L** and nitrogen of **phen** has been shown through the complexation process with Co(II), Cu(II), Y(III), Zr(IV) and La(III) which supported by spectroscopic data. The new mixed metal complexes have been characterized using spectroscopic and physicochemical techniques. The data supported the proposed coordination of six coordinated metal ions with distorted octahedral geometry formed by the ligands. The indicated molecular formulae of the complexes were supported by thermal studies, which also served to assess the stability of the compounds. In addition, the molar conductance statistics indicate that all complexes are electrolytic with chloride ions as counter ions. The antibacterial activity of each generated complex and the two parent ligands has been tested against a variety of food- and phytopathogen-causing microorganisms. In addition, complex (**5**) demonstrated significant activity against *C. albicans* compared to the parent ligands **L** and **phen** and other complexes.

Supplementary Materials: The following supporting information can be downloaded at <https://www.mdpi.com/article/10.3390/compounds3010022/s1>. Figure S1: Infrared spectra for **L**, **phen** and their metal complexes. Figure S2: Electronic absorption spectra for **L**, **phen** and their metal complexes. Figure S3: ¹H NMR spectra for **L**, **phen** and their metal complexes. Figure S4: TG and DTG diagrams for **L**, **phen** and their metal complexes.

Author Contributions: Conceptualization, H.S.E. and S.A.S.; formal analysis, A.A.N. and A.A.M.; investigation, H.S.E.; methodology, A.A.N. and A.A.M.; supervision, H.S.E. and S.A.S.; validation, A.A.N. and S.A.S.; visualization, A.A.M.; writing—original draft, H.S.E., A.A.N. and A.A.M.; writing—review and editing, S.A.S. All authors have read and agreed to the published version of the manuscript.

Funding: This research received no external funding.

Data Availability Statement: Not applicable.

Conflicts of Interest: The authors declare no conflict of interest.

References

1. Roat-Malone, R.M. *Bioinorganic Chemistry: A short Course*; John Wiley and Sons, Inc.: New York, NY, USA, 2002.
2. Crichton, R.R. *Biological Inorganic Chemistry an Introduction*; Elsevier: Amsterdam, The Netherlands, 2008.
3. Prakash, O.; Kumar, R.; Tyagi, P.; Kuhad, R.C. Organoiodine(III) mediated synthesis of 3,9-diaryl- and 3,9-difuryl-bis-1,2,4-triazolo[4,3-a][4,3-c]pyrimidines as antibacterial agents. *Eur. J. Med. Chem.* **2007**, *42*, 868–872. [[CrossRef](#)]
4. Zhang, N.; Ayrat-Kaloustian, S.; Nguyen, T.; Hernandez, R.; Beyer, C. 2-Cyanoaminopyrimidines as a class of antitumor agents that promote tubulin polymerization. *Bioorg. Med. Chem. Lett.* **2007**, *17*, 3003–3005. [[CrossRef](#)]
5. Lanier, M.C.; Feher, M.; Ashweek, N.J.; Loweth, C.J.; Rueter, J.K.; Slee, D.H.; Williams, J.P.; Zhu, Y.F.; Sullivan, S.K.; Brown, M.S. Selection, synthesis, and structure–activity relationship of tetrahydropyrido[4,3-d]pyrimidine-2,4-diones as human GnRH receptor antagonists. *Bioorg. Med. Chem.* **2007**, *15*, 5590–5603. [[CrossRef](#)]
6. EL-Shwiniy, W.A.; Ibrahim, A.G.; Sadeek, S.A.; Zordok, W.A. Synthesis, structural elucidation, molecular modeling and antimicrobial studies of 6-(2-hydroxyphenylimine)-2-thioxotetrahydropyrimidin-4 (1H)-one (L) Schiff base metal complexes. *Appl. Organomet. Chem.* **2021**, *35*, e6174. [[CrossRef](#)]
7. Abu-Dief, A.M.; El-khatib, R.M.; Aljohani, F.S.; Alzahrani, S.O.; Mahran, A.; Khalifa, M.E.; El-Metwaly, N.M. Synthesis and intensive characterization for novel Zn(II), Pd(II), Cr(III) and VO(II)-Schiff base complexes; DNA-interaction, DFT, drug-likeness and molecular docking studies. *J. Mol. Struct.* **2021**, *1242*, 130693. [[CrossRef](#)]
8. Munshi, A.M.; Bayazeed, A.A.; Abualnaja, M.; Morad, M.; Alzahrani, S.; Alkhatib, F.; Shah, R.; Zaky, R.; El-Metwaly, N.M. Ball-milling synthesis technique for Cu(II)-Schiff base complexes with variable anions; characterization, potentiometric study and in-vitro assay confirmed by in-silico method. *Inorg. Chem. Commun.* **2021**, *127*, 108542. [[CrossRef](#)]
9. Rajesh, P.; Gunasekaran, S.; Manikandan, A. Structural, spectral analysis of ambroxol using DFT methods. *J. Mol. Struct.* **2017**, *1144*, 379–388. [[CrossRef](#)]
10. Abd El-Hamid, S.M.; Sadeek, S.A.; El-Faragy, A.F.; Abd El-Lattif, N.S. Synthesis, structural characterization and ne-maticidal studies of some new N₂O₂ Schiff base metal complexes. *Bull. Chem. Soc. Ethiop.* **2021**, *35*, 315–335. [[CrossRef](#)]
11. Mahmoud, W.H.; Deghadi, R.G.; Mohamed, G.G. Metal complexes of novel Schiff base derived from iron sandwiched organometallic and 4-nitro-1,2-phenylenediamine: Synthesis, characterization, DFT studies, antimicrobial activities and molecular docking. *Appl. Organomet. Chem.* **2018**, *32*, e4289. [[CrossRef](#)]

12. Anacona, J.R.; Ruiz, K.; Loroño, M.; Celis, F. Antibacterial activity of transition metal complexes containing a tridentate NNO phenoxymethylpenicillin- based Schiff base. An anti-MRSA iron (II) complex. *Appl. Organomet. Chem.* **2019**, *33*, e47744. [[CrossRef](#)]
13. Golbedaghi, R.; Tabanez, A.M.; Esmaeili, S.; Fausto, R. Biological Applications of Macrocyclic Schiff Base Ligands and Their Metal Complexes: A Survey of the Literature(2005–2019). *Appl. Organomet. Chem.* **2020**, *34*, e5884. [[CrossRef](#)]
14. Mahmoud, W.H.; Omar, M.M.; Ahmed, Y.M.; Mohamed, G.G. Transition metal complexes of Schiff base ligand based on 4,6-diacetyl resorcinol. *Appl. Organomet. Chem.* **2020**, *34*, e5528. [[CrossRef](#)]
15. Jastrzab, R.; Kaczmarek, M.T.; Nowak, M.; Trojanowska, A.; Zabiszak, M. Complexes of polyamines and their derivatives as living system active compounds. *Coord. Chem. Rev.* **2017**, *351*, 32–44. [[CrossRef](#)]
16. Abd El-Hamid, S.M.; Sadeek, S.A.; Abd El-Lattif, N.S. Study of the chemical structure and their nematocidal activity of N₂O₂ tetradentate Schiff base metal complexes. *Appl. Organomet. Chem.* **2019**, *33*, e5010. [[CrossRef](#)]
17. Polarz, S.; Landsmann, S.; Klaiber, A. Hybrid Surfactant Systems with Inorganic Constituents. *Angew. Chem. Int. Ed.* **2014**, *53*, 946. [[CrossRef](#)]
18. Hubin, T.J.; Amoyaw, P.N.A.; Roewe, K.D.; Simpson, N.C.; Maples, R.D.; Freeman, T.N.C.; Cain, A.N.; Le, J.G.; Archibald, S.J.; Khan, S.I.; et al. Synthesis and antimalarial activity of metal complexes of cross-bridged tetraazamacrocyclic ligands. *Bioorg. Med. Chem.* **2014**, *22*, 3239. [[CrossRef](#)] [[PubMed](#)]
19. Khan, S.A.; Asiri, A.M.; Al-Amry, K.; Malik, M.A. Synthesis, Characterization, Electrochemical Studies, and In Vitro Antibacterial Activity of Novel Thiosemicarbazone and Its Cu(II), Ni(II), and Co(II) Complexes. *Sci. World J.* **2014**, *2014*, 592375. [[CrossRef](#)]
20. Ma, D.Y.; Zhang, L.X.; Rao, X.Y.; Wu, T.L.; Li, D.H.; Xie, X.Q.; Guo, H.F.; Qin, L. Structures, luminescence, and antibacterial studies of two transition metal complexes involving Schiff bases. *J. Coord. Chem.* **2013**, *66*, 3261. [[CrossRef](#)]
21. Kursunlu, A.N.; Guler, E.; Sevgi, F.; Ozkalp, B. Synthesis, spectroscopic characterization and antimicrobial studies of Co(II), Ni(II), Cu(II) and Zn(II) complexes with Schiff bases derived from 5-bromo-salicylaldehyde. *J. Mol. Struct.* **2013**, *1048*, 476. [[CrossRef](#)]
22. Keypour, H.; Shayesteh, M.; Rezaeivala, M.; Chalabian, F.; Elerman, Y.; Buyukgungor, O. Synthesis, spectral characterization, structural investigation and antimicrobial studies of mononuclear Cu(II), Ni(II), Co(II), Zn(II) and Cd(II) complexes of a new potentially hexadentate N₂O₄ Schiff base ligand derived from salicylaldehyde. *J. Mol. Struct.* **2013**, *1032*, 62. [[CrossRef](#)]
23. Dhanaraj, C.J.; Johnson, J.; Joseph, J.; Joseyphus, R.S. Quinoxaline-based Schiff base transition metal complexes: Review. *J. Coord. Chem.* **2013**, *66*, 1416. [[CrossRef](#)]
24. Ahmad, Z.; Chauhan, N.P.S.; Zarrintaj, P.; Khiabani, A.B.; Saeb, M.R.; Mozafari, M. Experimental procedures for assessing electrical and thermal conductivity of polyaniline. In *Fundamentals and Emerging Applications of Polyaniline*; Elsevier: Amsterdam, The Netherlands, 2019; Chapter 13; pp. 227–258.
25. de Souza, A.O.; Galetti, F.C.S.; Silva, C.L.; Bicalho, B.; Parma, M.M.; Fonscca, S.F. Antimycobacterial and cytotoxicity activity of synthetic and natural compounds. *Quim. Nova* **2007**, *30*, 6. [[CrossRef](#)]
26. Guo, Z.; Xing, R.; Liu, S.; Zhong, Z.; Ji, X.; Wang, L. Antifungal Properties of Schiff Bases of Chitosan, N-Substituted Chitosan and Quaternized Chitosan. *Carbohydr. Res.* **2007**, *342*, 1329–1332. [[CrossRef](#)]
27. Sadeek, S.A.; Abd El-Hamid, S.M. Synthesis spectroscopic, thermal analysis and in vitro biological properties of some new metal complexes with gemifloxacin and 1,10-phenanthroline. *J. Therm. Anal. Calorim.* **2016**, *124*, 547–562. [[CrossRef](#)]
28. Kucková, L.; Jomová, K.; Švorcová, A.; Valko, M.; Segl'a, P.; Moncol, J.; Kožíšek, J. Synthesis, crystal structure, spectroscopic properties and potential biological activities of salicylate–neocuproine ternary Copper(II) complexes. *Molecules* **2015**, *20*, 2115–2137. [[CrossRef](#)] [[PubMed](#)]
29. Salem, A.E.; Mohammed, S.F.; Sadeek, S.A.; Zordok, W.A.; El-Attar, M.S. Synthesis, structural elucidation, molecular modeling, and antimicrobial studies of some nanoparticles mixed ligands complexes of cetirizine in presence of 2,2'-bipyridine. *Appl. Organomet. Chem.* **2022**, *35*, e6715. [[CrossRef](#)]
30. Elshafie, H.S.; Sadeek, S.A.; Camele, I.; Mohamed, A.A. Biochemical characterization of new gemifloxacin schiff base (GMFX-ophdn) metal complexes and evaluation of their antimicrobial activity against some phyto- or human pathogens. *Int. J. Mol. Sci.* **2022**, *23*, 2110. [[CrossRef](#)]
31. Beecher, D.J.; Wong, A.C. Identification of hemolysin BL-producing *Bacillus cereus* isolates by a discontinuous hemolytic pattern in blood agar. *Appl. Environ. Microbiol.* **1994**, *60*, 1646. [[CrossRef](#)]
32. Elshafie, H.S.; Sakr, S.; Bufo, S.A.; Camele, I. An attempt of biocontrol the tomato-wilt disease caused by *Verticillium dahliae* using *Burkholderia gladioli* pv. *agaricicola* and its bioactive secondary metabolites. *Int. J. Plant Biol.* **2017**, *8*, 57–60. [[CrossRef](#)]
33. Sofo, A.; Elshafie, H.S.; Scopa, A.; Mang, S.M.; Camele, I. Impact of airborne zinc pollution on the antimicrobial activity of olive oil and the microbial metabolic profiles of Zn-contaminated soils in an Italian olive orchard. *J. Trace Elem. Med. Biol.* **2018**, *49*, 276–284. [[CrossRef](#)]
34. Wayne, P.A. *CLSI Document M07-A9; Methods for Dilutionantimicrobial Susceptibility Tests for Bacteria that Growaerobically*; Clinical and Laboratory Standard Institute: Wayne, NY, USA, 2012.
35. Geary, W.J. The use of conductivity measurements in organic solvents for the characterisation of coordination compounds. *Coord. Chem. Rev.* **1971**, *7*, 81–122. [[CrossRef](#)]
36. Abd El-Hamid, S.M.; Sadeek, S.A.; Mohammed, S.F.; Ahmed, F.M.; El-Gedamy, M.S. N₂O₂-chelate metal complexes with Schiff base ligand:Synthesis, characterisation and contribution as a promising antiviral agent against human cytomegalovirus. *Appl. Organomet. Chem.* **2023**, *37*, e6958. [[CrossRef](#)]

37. Elshafie, H.S.; Sadeek, S.A.; Camele, I.; Awad, H.M.; Mohamed, A.A. Biological and Spectroscopic Investigations of New Tenoxicam and 1.10-Phenthroline Metal Complexes. *Molecules* **2020**, *25*, 1027. [[CrossRef](#)] [[PubMed](#)]
38. Sadeek, S.A.; Mohamed, A.A. Ligational and biological studies of Fe(III), Co(II), Ni(II), Cu(II), and Zr(IV) complexes with carbamazepine as antiepileptic drug. *Appl. Organomet. Chem.* **2021**, *35*, e6178.
39. EL Amame, M.; Bouhdada, M. Synthesis and Characterization of the mixed ligand Complexes [M (Ac) 2 (caf) 2] M = Ni (II), Co (II), Zn (II), [Cu2 (μ -Ac) 4 (caf) 2], Ac = CH₃COO⁻, caf = caffeine. *Int. J. Chemtech. Res.* **2014**, *6*, 1430.
40. Rentschler, E.; Von Malotki, C. Spin transition in three-dimensional bridged coordination polymers of iron(II)-urea-triazoles. *Inorg. Chim. Acta* **2008**, *361*, 3646. [[CrossRef](#)]
41. Dilip, C.S.; Kumar, V.S.; Venison, S.J.; Potheher, I.V.; Subahashini, D.R. Synthesis, structural characterisation, bio-potential efficiency and DNA cleavage applications of nicotinamide metal complexes. *J. Mol. Struct.* **2013**, *1040*, 192–205. [[CrossRef](#)]
42. El-Ghamry, M.A.; Saleh, A.A.; Khalil, S.M.E.; Mohammed, A.A. Mono, bi- and trinuclear metal complexes derived from new benzene-1,4-bis(3-pyridin-2-ylurea) ligand. Spectral, magnetic, thermal and 3D molecular modeling studies. *Spectrochim. Acta A* **2013**, *110*, 205–216. [[CrossRef](#)]
43. Hassan, W.M.I.; Badawy, M.A.; Mohamed, G.G.; Moustafa, H.; Elramly, S. Synthesis, spectroscopic, thermal and DFT calculations of 2-(3-amino-2-hydrazone-4-oxothiazolidin-5-yl) acetic acid binuclear metal complexes. *Spectrochim. Acta A* **2013**, *111*, 169–177. [[CrossRef](#)]
44. Yousef, T.A.; Abu El-Reash, G.M.; El-Gammal, O.A.; Bedier, R.A. Synthesis, characterization, optical band gap, in vitro antimicrobial activity and DNA cleavage studies of some metal complexes of pyridyl thiosemicarbazone. *J. Mol. Struct.* **2013**, *1035*, 307–317. [[CrossRef](#)]
45. Uivarosi, V. Metal Complexes of Quinolone Antibiotics and Their Applications: An Update. *Molecules* **2013**, *18*, 11153–11197. [[CrossRef](#)]
46. Jena, V. *Electronic Spectra of Transition Metal Complexes*; Lulu Press Inc.: New York, NY, USA, 2015.
47. Cotton, F.A.; Wilkinson, G.; Murillo, C.A.; Bochmann, M. *Advanced Inorganic Chemistry*, 6th ed.; Wiley: New York, NY, USA, 1999.
48. Sadeek, S.A.; EL-Shwiniy, W.H. Metal complexes of the third generation quinolone antibacterial drug sparfloxacin: Preparation, structure, and microbial evaluation. *J. Coord. Chem.* **2010**, *63*, 3471. [[CrossRef](#)]
49. Macias, B.; Martinez, M.; Sanchez, A.; Dominguez-Gil, A.A. Physico-chemical study of the interaction of ciprofloxacin and ofloxacin with polivalentcations. *Int. J. Pharm.* **1994**, *106*, 229–235.
50. Elshafie, H.S.; Mohamed, A.A.; Sadeek, S.A.; Zordok, W.A. Meloxicam and Study of Their Antimicrobial Effects Against Phyto- and Human Pathogens. *Molecule* **2021**, *26*, 1480. [[CrossRef](#)]
51. Mohamed, A.A.; Ahmed, F.M.; Zordok, W.A.; EL-Shwiniy, W.H.; Sadeek, S.A.; Elshafie, H.S. Novel Enrofloxacin Schiff Base Metal Complexes: Synthesis, Spectroscopic Characterization, Computational Simulation and Antimicrobial Investigation against Some Food and Phyto-Pathogens. *Inorganics* **2022**, *10*, 177. [[CrossRef](#)]
52. Sadeek, S.A.; Abd El-Hamid, S.M. Preparation, characterization and cytotoxicity studies of some transition metal complexes with ofloxacin and 1,10-phenanthroline mixed ligand. *J. Mol. Struct.* **2016**, *1122*, 175–185. [[CrossRef](#)]
53. Ringer, A.L.; Sherrill, C.D.; King, R.A.; Crawford, T.D. Low-lying singlet excited states of isocyanogen. *Int. J. Quant. Chem.* **2008**, *108*, 1137–1140. [[CrossRef](#)]
54. Hoban, D.J.; Bouchillon, S.K.; Johnson, J.L.; Zhanel, G.G.; Butler, D.L.; Miller, L.A. Poupard JA Comparative in vitro activity of gemifloxacin, ciprofloxacin, levofloxacin and ofloxacin in a North American surveillance study. *Diagn. Microbiol. Infect. Dis.* **2001**, *40*, 51–57. [[CrossRef](#)]
55. Fernández-Roblas, R.; Cabria, F.; Esteban, J.; López, J.C.; Gadea, I.; Soriano, F. In vitro activity of gemifloxacin (SB 265805) compared with 14 other antimicrobials against intestinal pathogens. *J. Antimicrob. Chemother.* **2000**, *46*, 1023–1027. [[CrossRef](#)]
56. Elshafie, H.S.; Camele, I.; Sofo, A.; Mazzone, G.; Caivano, M.; Masi, S.; Caniani, D. Mycoremediation effect of *Trichoderma harzianum* strain T22 combined with ozonation in diesel-contaminated sand. *Chemosphere* **2020**, *252*, 126597. [[CrossRef](#)]
57. Saravolatz, L.; Manzor, O.; Check, C.; Pawlak, J.; Belian, B. Antimicrobial activity of moxifloxacin, gatifloxacin, and six fluoroquinolones against *Streptococcus pneumoniae*. *J. Antimicrob. Chemother.* **2001**, *47*, 875. [[CrossRef](#)]
58. Cottagnoud, P.; Acosta, F.; Cottagnoud, M.; Tauber, M.G. Gemifloxacin is efficacious against penicillin-resistant and quinolone-resistant pneumococci in experimental meningitis. *Antimicrob. Agents Chemother.* **2002**, *46*, 1607–1609. [[CrossRef](#)] [[PubMed](#)]
59. Sakr, S.H.; Elshafie, H.S.; Camele, I.; Sadeek, S.A. Synthesis, Spectroscopic, and Biological Studies of Mixed Ligand Complexes of Gemifloxacin and Glycine with Zn(II), Sn(II), and Ce(III). *Molecules* **2018**, *23*, 1182. [[CrossRef](#)] [[PubMed](#)]
60. Scheld, W.M. Maintaining fluoroquinolone class efficacy: Review of influencing factors. *Emerg. Infect. Dis.* **2003**, *9*, 1–9. [[CrossRef](#)] [[PubMed](#)]

Disclaimer/Publisher's Note: The statements, opinions and data contained in all publications are solely those of the individual author(s) and contributor(s) and not of MDPI and/or the editor(s). MDPI and/or the editor(s) disclaim responsibility for any injury to people or property resulting from any ideas, methods, instructions or products referred to in the content.